

STABILITY ANALYSIS FOR NONLINEAR SCHRÖDINGER EQUATIONS WITH NONLINEAR ABSORBING BOUNDARY CONDITIONS*

Jiwei Zhang

Applied and Computational Mathematics Division, Beijing Computational Science Research Center, China

Email: jwzhang@csrc.ac.cn

Zhenli Xu

Department of Mathematics, Institute of Natural Sciences, and MOE Key Lab of Scientific and Engineering Computing, Shanghai Jiao Tong University, Shanghai 200240, China

Email: xuzl@sjtu.edu.cn

Xiaonan Wu

Department of Mathematics, Hong Kong Baptist University, Kowloon, Hong Kong, China

Email: xwu@hkbu.edu.hk

Desheng Wang

Division of Mathematical Sciences, School of Physical and Mathematical Sciences, Nanyang Technological University, Singapore 637371, Singapore

Email: desheng@ntu.edu.sg

Abstract

Local absorbing boundary conditions (LABCs) for nonlinear Schrödinger equations have been constructed in papers [PRE 78(2008) 026709; and PRE 79 (2009) 046711] using the so-called unified approach. In this paper, we present stability analysis for the reduced problem with LABCs on the bounded computational domain by the energy estimate, and discuss a class of modified versions of LABCs. To prove the stability analysis of the reduced problem, we turn to the technique of some auxiliary variables which reduces the higher-order derivatives in LABCs into a family of equations with lower-order derivatives. Furthermore, we extend the strategy to the stability analysis of two-dimensional problems by carefully dealing with the LABCs at corners. Numerical examples are given to demonstrate the effectiveness of our boundary conditions and validate the theoretical analysis.

Mathematics subject classification: 65M12, 65M06, 65M15.

Key words: Nonlinear Schrödinger equations, Energy estimates, Absorbing boundary conditions.

1. Introduction

In this paper we consider numerical solutions of nonlinear Schrödinger (NLS) equations for wave function $\psi(x, t)$, given by

$$i\partial_t\psi(x, t) = -\Delta\psi(x, t) + f(|\psi|, x, t)\psi(x, t), \quad x \in \mathbb{R}^d, \quad t > 0, \quad (1.1)$$

with $d = 1, 2$. The nonlinear Schrödinger equation has been widely studied in fluid mechanics, nonlinear optics, atomic and molecular physics, for which, the nonlinear term $f(|\psi|, x, t)$ could

* Received April 7, 2014 / Revised version received August 27, 2016 / Accepted August 28, 2016 /
Published online January 18, 2017 /

have different forms depending on practical applications [1–4]. For example, in fluid mechanics and optics, it usually appears as a cubic nonlinear Schrödinger (NLS) equation. In Bose-Einstein condensation [5], Eq. (1.1) is known as the Gross-Pitaevskii equation, where $f(|\psi|, x, t)$ is composed of a nonlinear potential and a harmonic trap potential. Recent interest of this class of Schrödinger equations also includes the time-dependent density functional theory [6] to investigate quantum many-body systems, for which the potential comes from the external field and the internal Coulomb interactions.

The wave function in the NLS equation is defined on an infinite domain. The design of suitable boundary conditions is essential for numerical computations on an interested truncated region, which is the main concern of the present work. Historically, the so-called absorbing (or artificial) boundary condition (ABC) has been widely studied for various types of linear PDEs for which the classical techniques such as the Fourier (Laplace) transform and the spherical harmonics expansion, are usually applicable (see recent reviews [7–9]). However, it is notoriously hard for treating nonlinear equations due to the lack of general tools, presenting an urgent requirement for people working on this field to develop new techniques and methodologies.

Some useful methods have been developed for designing ABCs of NLS equations. A class of these methods are by considering the physical material near the boundary as an artificial potential which absorbs outgoing waves. One technique is the perfectly matched layer (PML) [10–12], which had been applied to numerically solve NLS equations [13, 14]. Another material-based method [15] is to add a negative imaginary potential as absorbing potential to the model equation, which has been often used in practical simulations.

Mathematically, there are two types of ABCs, say, nonlocal and local ABCs, which have been developed to treat both linear and nonlinear Schrödinger equations. For linear equations, the nonlocal condition, also called the transparent condition or DtN map, is exact and of integral form in time, and has been studied from different aspects such as analysis of discretization schemes [16], fast evaluation of the integral [17] and extension to multi-dimensions [18, 19]. The exact ABCs for NLS equations are only available for some very special cases, limited to one-dimensional version. A typical example is the integrable cubic NLS equation, which can be solved by the inverse scattering method [20]. Also, if the potential $f(|\psi|, x, t)$ is independent of the wave function and periodic outside the computational domain, efficient methods were developed in recent papers to construct exact ABCs (see, for example, [21, 22] and reference therein). For a general potential, it is well-known that one could not solve out an explicit representation of ABCs, since nonlinear interaction and the wave-potential interaction are too complex to clearly understand, and thus some simplification has to be applied. Under the assumption that the potential is slowly oscillatory and the density wave is of high-frequency propagation, a general approach [23–25] has been developed by extending the result of linear versions, and tested for many different potentials.

Local ABCs (LABCs) are usually constructed by extending the classical Engquist-Majda method [26] to factorize the Schrödinger operator in the linear equation, and to approximate the outgoing component by the Taylor or Padé expansions. The obtained differential equations can be naturally coupled with the nonlinear term by the time-splitting technique [28, 29], which results in ABCs in discretization form. Recently, this approach was further developed into a general principle, called the unified approach [30–32], by recombining the subproblems of the time-splitting procedure into a continuous nonlinear differential equations as the effective LABCs. With these LABCs, the problem on unbounded domain is reformulated into a reduced problem on a bounded domain. To our knowledge, a rigorous mathematical analysis of the

stability and accuracy of the reduced problem remains open, namely,

1. What is the approximate accuracy of the reduced problem with LABCs to the original problem?
2. What is the stability of the reduced problem with LABCs in energy estimate?

The aim of this paper focuses on the second problem. We analyze the stability of the reduced problems with the obtained LABCs in [30, 31], and systematically validate the performance of boundary conditions by numerical examples with various nonlinear and complex potentials. By introducing the auxiliary-variables, the obtained LABCs with higher-order mixed derivatives are reduced into a family of equations with lower-order derivatives. Furthermore, the strategy is extended to two-dimensional case by carefully dealing with the boundary condition at corners. The initial-boundary-value (IBV) problems with LABCs proposed in [30, 31] are proven to be theoretically stable in L^2 -norm. In addition, a variety of boundary conditions (2.11) is also obtained by the unified approach, and have a better performance than the boundary conditions in [30] by numerically comparing the L^2 -errors and normalized L^2 -norm. However, the stability analysis of problems with these boundary conditions remains open.

The organization of this paper is as follows. In Section 2, we discuss the unified approach for one-dimensional NLS equations. By turning to some auxiliary variables to avoid the mixed partial derivatives in LABCs, the stability analysis of the reduced IBV problem is given. In Section 3, the stability analysis is extended to two-dimensional cases, and the difficulty of boundary conditions at corners is circumvented. Section 4 shows an efficient discretization scheme and presents numerical examples to demonstrate the accuracy and effectiveness of the obtained boundary conditions. We end the paper with the conclusion.

2. Boundary Conditions and Stability Analysis in 1D

In this section, we discuss the construction of the LABCs and the stability of resulted IBV problems for one-dimensional NLS equations. The interior domain of computational domain is defined by $\Omega_i :=]x_l, x_r[$. And $\bar{\Omega}_i$ denotes the closure of the set Ω_i and the boundary denotes $\Gamma := \{x_l, x_r\}$.

2.1. Unified approach: general principle

Before embarking on the design of LABCs, we briefly recall the philosophy of the unified approach and rewrite equation (1.1) in the operator form

$$i\partial_t\psi = \mathcal{L}\psi + \mathcal{N}\psi \quad (2.1)$$

with $\mathcal{L}\psi := -\Delta\psi$ and $\mathcal{N}\psi := f(|\psi|, x, t)\psi$. Over a time interval from t to $t + \tau$ for small τ , in analog to the Strang's splitting method [34], the approximation

$$\psi(x, t + \tau) \approx e^{-i\tau\mathcal{L}}e^{-i\tau\mathcal{N}}\psi(x, t) \quad (2.2)$$

is used. We replace the linear operator \mathcal{L} by a one-directional approximation operator $\mathcal{L}^{(n)}$ (make the waves outgoing), then combine $\mathcal{L}^{(n)}$ with the nonlinear term \mathcal{N} . We restrict (2.2) to artificial boundaries and obtain the following expression

$$i\partial_t\psi(x, t) = \mathcal{L}^{(n)}\psi(x, t) + \mathcal{N}\psi(x, t), \quad (2.3)$$

as the nonlinear absorbing boundary condition. The superscript n is related to the convergence rate of the Padé expansion. How to obtain a good approximation $\mathcal{L}^{(n)}$ plays an important role in the quality of the ABCs.

2.2. Construction of nonlinear absorbing boundary conditions

To construct the approximation operator $\mathcal{L}^{(n)}$, we first consider one-dimensional linear Schrödinger equation

$$i\psi(x, t) = -\partial_x^2 \psi(x, t) = \mathcal{L}\psi(x, t). \quad (2.4)$$

Assume that the artificial boundaries are transparent to a plane wave in the form of $\psi(x, t) = \exp[-i(\omega t - \xi x)]$, where ω is the frequency and ξ is the wave number. Substituting the plane wave form into Eq. (2.4), one obtains the corresponding dispersion relation $\xi^2 = \omega$, and solves it to yield

$$\xi = \pm\sqrt{\omega}, \quad (2.5)$$

where the plus and minus signs correspond to the right- and left-going waves, respectively. Under the framework of Engquist and Majda's approach [27], we expand Eq. (2.5) at point ω_0 by a rational polynomial, to obtain

$$\sqrt{\omega} \approx \sqrt{\omega_0} - \sqrt{\omega_0} \sum_{m=1}^N \frac{b_m (\omega_0 - \omega)}{\omega_0 - a_m (\omega_0 - \omega)}, \quad (2.6)$$

where

$$a_m = \cos^2 \left(\frac{m\pi}{2N+1} \right), \quad b_m = \frac{2}{2N+1} \sin^2 \left(\frac{m\pi}{2N+1} \right), \quad m = 1, \dots, N.$$

Substituting the Padé expansion (2.6) into (2.5) with $k_0 = \sqrt{\omega_0}$, we have

$$\xi = \pm k_0 \left(1 - \sum_{m=1}^N \frac{b_m (k_0^2 - \omega)}{k_0^2 - a_m (k_0^2 - \omega)} \right). \quad (2.7)$$

The approximation (2.7) is called the paraxial approximation in literature. Taking $N = 1$, and applying the dual relation $\xi \Leftrightarrow -i\partial_x$ and $\omega \Leftrightarrow i\partial_t$, we have the third-order ABCs

$$-\psi_{xt} \pm 3ik_0\psi_t + 3ik_0^2\psi_x \pm k_0^3\psi = 0, \quad (2.8)$$

which reproduce the Kuska's boundary conditions [33]. The "third-order" represents the convergence rate of the Padé approximation. We rewrite Eq. (2.8) in the form of

$$i\partial_t \psi = -(i\partial_x \pm 3k_0)^{-1} (3ik_0^2\partial_x \pm k_0^3) \psi := \mathcal{L}^{(3)}\psi. \quad (2.9)$$

Comparing linear Schrödinger equation (2.4) with approximated equations (2.9), we can consider $\mathcal{L}^{(3)}$ as an approximation of \mathcal{L}

$$\mathcal{L} \approx \mathcal{L}^{(3)} := -(i\partial_x \pm 3k_0)^{-1} (3ik_0^2\partial_x \pm k_0^3). \quad (2.10)$$

Substituting (2.10) into (2.3) leads us to the nonlinear LABCs for the NLS equation,

$$-\psi_{xt} \pm 3ik_0\psi_t + 3ik_0^2\psi_x \pm k_0^3\psi = f(|\psi|, x, t) (i\psi_x \pm 3k_0\psi) + if(|\psi|, x, t)_x \psi. \quad (2.11)$$

The boundary conditions obtained in [30, 31] are

$$-\psi_{xt} \pm 3ik_0\psi_t + 3ik_0^2\psi_x \pm k_0^3\psi = f(|\psi|, x, t) (i\psi_x \pm 3k_0\psi). \quad (2.12)$$

One can see that there is one more term $if(|\psi|, x, t)_x\psi$ in (2.11) than (2.12). We remark that if the amplitudes of $f(|\psi|, x, t)_x\psi$ is small enough, the two boundary conditions have tiny difference, and can be considered as a variety of each other. In fact, the boundary condition (2.12) is derived under an assumption that the potential is slowly oscillatory or the waves are with high frequency, by which the reflection waves are weak, and there are only minor reflection waves in comparison to the outgoing waves. Accordingly, the nonlinear term and potential can be approximately taken as constants over small time step, thus $f(|\psi|, x, t)_x\psi$ vanishes over each time step. From this viewpoint, it is vivid to call boundary conditions (2.12) the linearized LABCs although they are indeed nonlinear in the form. To differ from boundary conditions (2.12), we will keep the notation of linearized LABCs if it does not cause any confusion. For brevity, we express LABCs (2.11) and linearized LABCs (2.12):

$$\mathcal{L}ABC_{\pm}(x, t, \psi(x, t)) = 0,$$

$$\mathcal{L}\mathcal{L}ABC_{\pm}(x, t, \psi(x, t)) = 0,$$

where $\mathcal{L}ABC_{-}$ (or $\mathcal{L}\mathcal{L}ABC_{-}$) and $\mathcal{L}ABC_{+}$ (or $\mathcal{L}\mathcal{L}ABC_{+}$) represent the left and right boundary conditions, respectively. In this paper, we consider the stability of the reduced problems obtained in [30, 31], namely,

$$\begin{cases} i\partial_t\psi = -\partial_x^2\psi + f(|\psi|, x, t)\psi, & x \in \Omega_i, \\ \mathcal{L}\mathcal{L}ABC_{\pm}(x, t, \psi(x, t)) = 0, & x \in \Gamma, \\ \psi(x, 0) = \psi_0(x), & x \in \Omega_i. \end{cases} \quad (2.13)$$

It should be pointed out that the physical parameter k_0 in boundary conditions (2.11) and (2.12) is essential for the accuracy of approximating the dispersion relation (2.5). The choice of parameter $k_0 = \sqrt{w_0}$ is related to the frequency of wave impinging on the artificial boundaries, and the Padé approximation to the dispersion relation (2.6) at the expansion point w_0 would be more accurate when w_0 is closer to the real frequency w . Furthermore, the relation between group velocity C and wavenumber k is given by $C = \frac{\partial\omega}{\partial k} = 2k$. Thus the parameters k_0 is a finite positive number since the group velocity of wave is considered to be finite in this paper. To be more accurate, the parameters should be determined adaptively [29]; see Appendix for a detailed description.

2.3. Stability analysis for one dimensional problem

In order to prove the stability of the reduced problem (2.13), we reconstruct the derivation of boundary conditions (2.12). This proposal will give some hints how to circumvent the difficulty of mixed derivatives. Under an assumption that the potential is slowly oscillatory, the nonlinear term and potential can be approximately taken as constants over small time step. Thus the dispersion relation of model equation is given by $\xi^2 = \omega - f$ and the one-way relations are

$$\xi = \pm\sqrt{\omega - f}. \quad (2.14)$$

Denoting $z = \omega - f$ and using the expansion (2.6) for $N = 1$ at point z_0 , we have

$$\xi = \pm\sqrt{\omega - f} \approx \pm\sqrt{z_0} \frac{z_0 + 3z}{3z_0 + z} = \pm\sqrt{z_0} \left(3 - \frac{8z_0}{3z_0 + \omega - f} \right). \quad (2.15)$$

The formulas can be rearranged into

$$\xi (3k_0^2 + \omega - f) = \pm k_0 (k_0^2 + 3\omega - 3f) \quad (2.16)$$

with $k_0 = \sqrt{z_0}$. Multiplying both side of (2.16) by ψ and applying the duality $\xi \Leftrightarrow -i\partial_x$ and $\omega \Leftrightarrow i\partial_t$, the so-called $\mathcal{L}\mathcal{L}\mathcal{A}\mathcal{B}\mathcal{C}$ s (2.12) are achieved. To circumvent the mixed derivatives, we multiply both sides of (2.15) by ψ , introduce the auxiliary variables

$$\phi_l = \frac{1}{3k_0^2 + \omega - f} \psi,$$

and arrive at

$$\begin{cases} \xi\psi = \pm k_0(3\psi - 8k_0^2\phi_l) \\ (3k_0^2 + \omega - f)\phi_l = \psi, \end{cases} \quad (2.17)$$

with $l = 1, 2$, where $l = 1$ represents the auxiliary variable at the left boundary, and $l = 2$ represents at the right boundary. By applying the dual relation $\xi \Leftrightarrow -i\partial_x$ and $\omega \Leftrightarrow i\partial_t$ to (2.17), the boundary conditions (2.12) are equivalently rewritten as

$$\begin{cases} i\partial_x\psi \pm k_0(3\psi - 8k_0^2\phi_l(t)) = 0, \\ 3k_0^2\phi_l(t) + i\partial_t\phi_l(t) - \phi_l(t)f(|\psi|, x, t) = \psi. \end{cases} \quad (2.18)$$

Thus the reduced problem (2.13) is equivalent to

$$\begin{cases} i\partial_t\psi = -\partial_x^2\psi + f(|\psi|, x, t)\psi, & x_l < x < x_r, \quad 0 < t \leq T, \\ i\partial_x\psi(x_l, t) - k_0(3\psi(x_l, t) - 8k_0^2\phi_1(t)) = 0, \\ i\partial_x\psi(x_r, t) + k_0(3\psi(x_r, t) - 8k_0^2\phi_2(t)) = 0, \\ 3k_0^2\phi_1(t) + i\partial_t\phi_1(t) - f(|\psi|, x_l, t)\phi_1(t) = \psi(x_l, t), \\ 3k_0^2\phi_2(t) + i\partial_t\phi_2(t) - f(|\psi|, x_r, t)\phi_2(t) = \psi(x_r, t), \\ \psi(x, 0) = \psi_0(x), \quad x_l \leq x \leq x_r; \quad \phi_1(0) = 0, \quad \phi_2(0) = 0. \end{cases} \quad (2.19)$$

Theorem 2.1. *Assume that $f(|\psi|, x, t)$ is a real function. Let $\psi(x, t)$ be the solution of (2.19). We have*

$$\|\psi\|_{\Omega_i}^2 + 8k_0^3 \left(|\phi_1(t)|^2 + |\phi_2(t)|^2 \right) \leq e^{\frac{8k_0^2 t}{3}} \|\psi_0\|_{\Omega_i}^2, \quad 0 < t \leq T. \quad (2.20)$$

Proof. Multiplying the first equation in (2.19) by $\bar{\psi}(x, t)$, integrating by parts over $[x_l, x_r]$, taking the imaginary part and noting that $f(|\psi|, x, t)$ is real, we have

$$\frac{1}{2} \frac{d}{dt} \|\psi\|_{\Omega_i}^2 = \text{Im} \left\{ \bar{\psi}(x_l, t) \partial_x \psi(x_l, t) - \bar{\psi}(x_r, t) \partial_x \psi(x_r, t) \right\}. \quad (2.21)$$

Inserting the second and third equations of (2.19) into (2.21), we get

$$\frac{1}{2} \frac{d}{dt} \|\psi\|_{\Omega_i}^2 = -3k_0 \left(|\psi(x_l, t)|^2 + |\psi(x_r, t)|^2 \right) + 8k_0^3 \text{Re} \left\{ \bar{\psi}(x_l, t) \phi_1(t) + \bar{\psi}(x_r, t) \phi_2(t) \right\}. \quad (2.22)$$

Multiplying the fourth equation of (2.19) by $\bar{\phi}_{m,1}(t)$, leads to

$$3k_0^2 |\phi_1(t)|^2 + i\bar{\phi}_1(t)\partial_t\phi_1(t) - f(|\psi|, x_l, t) |\phi_1(t)|^2 = \bar{\phi}_1(t)\psi(x_l, t).$$

Using $\text{Im}\{f(|\psi|, x, t)\} = 0$ and taking the imaginary part, and multiplying the resulting by $8k_0^3$, we obtain

$$4k_0^3 \frac{d}{dt} |\phi_1(t)|^2 = 8k_0^3 \text{Im} \{ \psi(x_l, t) \bar{\phi}_1(t) \}. \quad (2.23)$$

Similarly, for the fifth equation of (2.19), we can obtain

$$4k_0^3 \frac{d}{dt} |\phi_2(t)|^2 = 8k_0^3 \text{Im} \{ \psi(x_r, t) \bar{\phi}_2(t) \}. \quad (2.24)$$

Adding (2.22), (2.23) and (2.24) together, we get

$$\begin{aligned} & \frac{1}{2} \frac{d}{dt} \left\{ \|\psi\|_{\Omega_i}^2 + 8k_0^3 \left(|\phi_1(t)|^2 + |\phi_2(t)|^2 \right) \right\} \\ &= -3k_0 \left(|\psi(x_l, t)|^2 + |\psi(x_r, t)|^2 \right) + 8k_0^3 \text{Re} \{ \psi(x_l, t) \bar{\phi}_1(t) + \psi(x_r, t) \bar{\phi}_2(t) \} \\ & \quad + 8k_0^3 \text{Im} \{ \psi(x_l, t) \bar{\phi}_1(t) + \psi(x_r, t) \bar{\phi}_2(t) \}. \end{aligned} \quad (2.25)$$

Using $|\text{Re}(Z)| + |\text{Im}(Z)| \leq \sqrt{2} |Z|$ and the ϵ inequality, i.e. $ab \leq \epsilon a^2 + \frac{b^2}{4\epsilon}$, we have

$$\begin{aligned} A &\equiv 8k_0^3 \text{Re} \{ \psi(x_l, t) \bar{\phi}_1(t) + \psi(x_r, t) \bar{\phi}_2(t) \} + 8k_0^3 \text{Im} \{ \psi(x_l, t) \bar{\phi}_1(t) + \psi(x_r, t) \bar{\phi}_{m,2}(t) \} \\ &\leq 8\sqrt{2}k_0^3 \left(|\psi(x_l, t) \bar{\phi}_1(t)| + |\psi(x_r, t) \bar{\phi}_2(t)| \right) \\ &\leq \epsilon \left(|\psi(x_l, t)|^2 + |\psi(x_r, t)|^2 \right) + \frac{32k_0^6}{\epsilon} \left(|\bar{\phi}_1(t)|^2 + |\bar{\phi}_2(t)|^2 \right). \end{aligned} \quad (2.26)$$

Taking $\epsilon = 3k_0$, we arrive at

$$A \leq 3k_0 \left(|\psi(x_l, t)|^2 + |\psi(x_r, t)|^2 \right) + \frac{32k_0^5}{3} \left(|\phi_1(t)|^2 + |\phi_2(t)|^2 \right).$$

Inserting above inequality into (2.25), we obtain

$$\frac{d}{dt} \left\{ \|\psi\|_{\Omega_i}^2 + 8k_0^3 \left(|\phi_1(t)|^2 + |\phi_2(t)|^2 \right) \right\} \leq \frac{8k_0^2}{3} \cdot 8k_0^3 \left(|\phi_1(t)|^2 + |\phi_2(t)|^2 \right).$$

Gronwall inequality yields (2.20). This completes the proof. \square

In Theorem 2.1, the parameter k_0 is considered as a finite positive constant. In fact, the parameter k_0 is often chosen such that they are close to the group velocity of the wave impinging on the artificial boundaries, the parameter k_0 will change with time t . One can see the adaptive selection of the parameter k_0 by formula (A.2) in Appendix. When $k_0(t) \neq 0$ for $t \in [0, T]$, by changing Eqs. (2.23) and (2.24), we will have a rough result (instead of Eq. (2.20)) as

$$\|\psi\|_{\Omega_i}^2 + \left(|\phi_1(t)|^2 + |\phi_2(t)|^2 \right) \leq e^{\int_0^t \frac{8(k_0^3(\tau)+1)^2}{3k_0(\tau)} d\tau} \|\psi_0\|_{\Omega_i}^2, \quad 0 < t \leq T. \quad (2.27)$$

Since $k_0(t)$ depends on the finite velocities of wave impinging on the artificial boundary, we can take the maximum of $k_0(t)$ by $k_0^m = \max_{0 < t \leq T} \{k_0(t)\}$ and have:

$$\|\psi\|_{\Omega_i}^2 + \left(|\phi_1(t)|^2 + |\phi_2(t)|^2 \right) \leq e^{\frac{8((k_0^m)^3+1)^2}{3k_0^m} t} \|\psi_0\|_{\Omega_i}^2, \quad 0 < t \leq T. \quad (2.28)$$

We end this section with a remark that when the adaptive selection of k_0 is applied, the k_0 can be chosen zero when the wave has not touched the artificial boundaries. In this situation, the boundary conditions are equivalent to a zero boundary condition, hence we can take any finite positive k_0 with the same effects. The same remark is suitable for Theorem 3.1 for the case of $\eta_0 = 0$ and $\xi_0 = 0$.

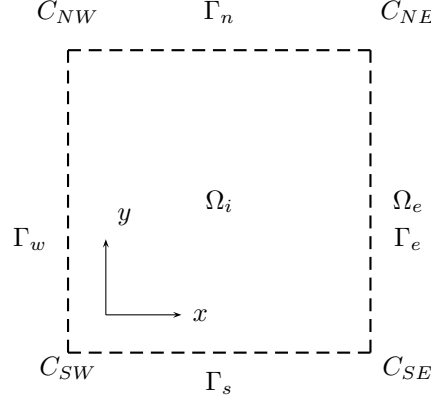


Fig. 2.1. Settings of unbounded problems.

3. Boundary Conditions and Stability Analysis in 2D

We have obtained the stability of the reduced IBV problem for 1D spatial domain, which motivates us to apply the spirit to 2D case. As showed in Fig. 2.1, the artificial boundaries are defined by

$$\begin{aligned} \Gamma_e &= \{(x, y) | x = L, 0 \leq y \leq L\}, & \Gamma_w &= \{(x, y) | x = 0, 0 \leq y \leq L\}, \\ \Gamma_n &= \{(x, y) | 0 \leq x \leq L, y = L\}, & \Gamma_s &= \{(x, y) | 0 \leq x \leq L, y = 0\}, \end{aligned}$$

which divide the unbounded domain \mathbb{R}^2 into two parts: the bounded (interior) domain Ω_i and unbounded (exterior) domain Ω_e , namely,

$$\Omega_i = \{(x, y) | 0 < x < L, 0 < y < L\}, \quad \text{and} \quad \Omega_e = \mathbb{R}^2 \setminus \bar{\Omega}_i.$$

Zhang et al. [31] constructed the corresponding LABCs for two-dimensional NLS equations, and proposed the treatment of boundary conditions at corners. In this paper, we use the energy estimate to prove the stability of those boundary conditions. For a general initial compactly supported wave package, the wave has different group velocities, and will propagate along the same directions, and then impinges on the artificial boundaries. To avoid complicated notations (i.e., auxiliary variables), we assume that the solutions propagate into the northern-eastern corner C_{NE} . Thus we set LABCs on boundaries Γ_n , Γ_e and corner C_{NE} , and homogeneous Dirichlet boundary conditions on other parts of boundaries. Now we recall the boundary conditions of [31]: BC on Γ_e

$$-i3\xi_0^2 \partial_x \psi + \partial_x \partial_t \psi - i \partial_x \partial_y^2 \psi = \xi_0^3 \psi + 3i\xi_0 \partial_t \psi + 3\xi_0 \partial_y^2 \psi - f(|\psi|, x, t)(i \partial_x \psi + 3\xi_0 \psi); \quad (3.1)$$

BC on Γ_n

$$-i3\eta_0^2 \partial_y \psi + \partial_y \partial_t \psi - i \partial_y \partial_x^2 \psi = \eta_0^3 \psi + 3i\eta_0 \partial_t \psi + 3\eta_0 \partial_x^2 \psi - f(|\psi|, x, t)(i \partial_y \psi + 3\eta_0 \psi); \quad (3.2)$$

BC at C_{NE}

$$\begin{aligned}
& 3\xi_0\partial_y\partial_t\psi + 3\eta_0\partial_x\partial_t\psi + \left(3\xi_0^2 + 3\eta_0^2 - f(|\psi|, x, t)\right)\partial_x\partial_y\psi \\
& - i\xi_0\left(\xi_0^2 + 9\eta_0^2 - 3f(|\psi|, x, t)\right)\partial_y\psi + i\partial_x\partial_y\partial_t\psi - 9i\xi_0\eta_0\partial_t\psi \\
& - i\eta_0\left(\eta_0^2 + 9\xi_0^2 - 3f(|\psi|, x, t)\right)\partial_x\psi + 3\xi_0\eta_0\left(3f(|\psi|, x, t) - \xi_0^2 - \eta_0^2\right)\psi = 0, \tag{3.3}
\end{aligned}$$

where η_0 is the wave-number along x -direction and ξ_0 along y -direction. The parameters η_0 and ξ_0 are the expansion points of Padé approximation to the dispersion relation.

The model equation and initial value on Ω_i are rewritten by

$$i\partial_t\psi = -\Delta\psi + f(|\psi|, x, t)\psi, \quad (x, y) \in \Omega_i \tag{3.4}$$

$$\psi(x, y, 0) = \psi_0, \quad (x, y) \in \Omega_i. \tag{3.5}$$

For the reduced problem (3.1)-(3.5), the essential difficulty arises from the equation at corner C_{NE} , which can be considered as a bridge to connect ABCs between Γ_n and Γ_e . Similar to the aforementioned 1D case, auxiliary variables are introduced to reduce higher-order derivatives into a system of equations with lower-order derivatives. For BCs on Γ_e and Γ_n , namely, (3.1) and (3.2), the equivalent forms are respectively given by

$$2\xi_0^3\phi_1(y, t) = -i\partial_x\psi + 3\xi_0\psi, \tag{3.6}$$

$$3\xi_0^2\phi_1(y, t) + i\partial_t\phi_1(y, t) + \partial_y^2\phi_1(y, t) - f(|\psi|, x, t)\phi_1(y, t) = 4\psi, \tag{3.7}$$

$$2\eta_0^3\phi_2(x, t) = -i\partial_y\psi + 3\eta_0\psi, \tag{3.8}$$

$$3\eta_0^2\phi_2(x, t) + i\partial_t\phi_2(x, t) + \partial_x^2\phi_2(x, t) - f(|\psi|, x, t)\phi_2(x, t) = 4\psi. \tag{3.9}$$

For BC at corner C_{NE} (3.3), we define auxiliary variables Φ_1 and Φ_2 , and write them in equivalent forms of form is

$$\Phi_1(t) = i\partial_y\phi_1 + 3\eta_0\phi_1, \tag{3.10}$$

$$2i\partial_t\Phi_1 = -3(\eta_0^2 + \xi_0^2)\Phi_1 + 8\eta_0^3(\phi_1 + \phi_2) + 2f(|\psi|, x, t)\Phi_1, \tag{3.11}$$

or,

$$\Phi_2(t) = i\partial_x\phi_2 + 3\xi_0\phi_2, \tag{3.12}$$

$$2i\partial_t\Phi_2 = -3(\eta_0^2 + \xi_0^2)\Phi_2 + 8\xi_0^3(\phi_1 + \phi_2) + 2f(|\psi|, x, t)\Phi_2. \tag{3.13}$$

Since initial data ψ_0 is compactly supported, e.g., $\psi_0 = 0$ on the artificial boundaries, thus the initial values of those auxiliary variables are zero from the definitions of (3.6), (3.8), (3.10) and (3.12). Now we have the following theorem for the IBV problem (3.4)-(3.13).

Theorem 3.1. *Assume that $f(|\psi|, x, t)$ is a real function. Let $\psi(x, t)$ be the solution of the reduced problem (3.4)-(3.13) with the Dirichlet boundary conditions on Γ_w and Γ_e , and denote $c = \max\{8\xi_0^5/3, 8\eta_0^5/3, 2\xi_0^3/\eta_0, 2\eta_0^3/\xi_0\}$. We have*

$$\begin{aligned}
& \|\psi\|_{\Omega_i}^2 + \frac{1}{2}\left(\xi_0^3\|\phi_1\|_{[0, L]}^2 + \eta_0^3\|\phi_2\|_{[0, L]}^2\right) + \frac{\xi_0^3}{8\eta_0^3}|\Phi_1|^2 + \frac{\eta_0^3}{8\xi_0^3}|\Phi_2|^2 \\
& \leq e^{2ct}\|\psi_0\|_{\Omega_i}^2, \quad 0 < t \leq T. \tag{3.14}
\end{aligned}$$

Proof. Multiplying (3.4) by $\bar{\psi}$, integrating by parts on Ω_i , and taking the imaginary part, we have

$$\frac{1}{2} \frac{d}{dt} \|\psi\|_{\Omega_i}^2 = -\text{Im} \left\{ \int_0^L \bar{\psi}(L, y, t) \partial_x \psi(L, y, t) dy + \int_0^L \bar{\psi}(x, L, t) \partial_y \psi(x, L, t) dx \right\}. \quad (3.15)$$

Plugging (3.6) and (3.8) into (3.15), we obtain

$$\begin{aligned} \frac{1}{2} \frac{d}{dt} \|\psi\|_{\Omega_i}^2 &= -3 \left(\xi_0 \|\psi(L, y, t)\|_{[0, L]}^2 + \eta_0 \|\psi(x, L, t)\|_{[0, L]}^2 \right) \\ &\quad + 2\text{Re} \left\{ \xi_0^3 \int_0^L \bar{\psi} \phi_1 dy + \eta_0^3 \int_0^L \bar{\psi} \phi_2 dx \right\}. \end{aligned} \quad (3.16)$$

Multiplying (3.7) by $\bar{\phi}_1(t)$, integrating by parts over $[0, L]$ and taking the imaginary part, we have

$$\frac{\xi_0^3}{4} \frac{d}{dt} \|\phi_1\|_{[0, L]}^2 = -\frac{\xi_0^3}{2} \text{Im} \{ \bar{\phi}_1(L, L, t) \partial_y \phi_1(L, L, t) \} + 2\xi_0^3 \text{Im} \int_0^L \psi \bar{\phi}_1 dy.$$

Noting that $\partial_y \phi_1 = -i\Phi_1(t) + 3i\eta_0\phi_1$ from (3.10), we have

$$\frac{\xi_0^3}{4} \frac{d}{dt} \|\phi_1\|_{[0, L]}^2 = -\frac{3\xi_0^3\eta_0}{2} |\phi_1(L, L, t)|^2 + \frac{\xi_0^3}{2} \text{Re} \{ \bar{\phi}_1(L, L, t) \Phi_1(t) \} + 2\xi_0^3 \text{Im} \int_0^L \psi \bar{\phi}_1 dy. \quad (3.17)$$

Similarly,

$$\frac{\eta_0^3}{4} \frac{d}{dt} \|\phi_2\|_{[0, L]}^2 = -\frac{3\eta_0^3\xi_0}{2} |\phi_2(L, L, t)|^2 + \frac{\eta_0^3}{2} \text{Re} \{ \bar{\phi}_2(L, L, t) \Phi_2(t) \} + 2\eta_0^3 \text{Im} \int_0^L \psi \bar{\phi}_2 dx. \quad (3.18)$$

Multiplying (3.11) by $\bar{\Phi}_1(t)$, (3.13) by $\bar{\Phi}_2(t)$, and taking the imaginary part, lead us to

$$\frac{\xi_0^3}{16\eta_0^3} \frac{d}{dt} |\Phi_1|^2 = \frac{\xi_0^3}{2} \text{Im} \{ (\phi_1(L, L, t) + \phi_2(L, L, t)) \bar{\Phi}_1(t) \}, \quad (3.19)$$

$$\frac{\eta_0^3}{16\xi_0^3} \frac{d}{dt} |\Phi_2|^2 = \frac{\eta_0^3}{2} \text{Im} \{ (\phi_1(L, L, t) + \phi_2(L, L, t)) \bar{\Phi}_2(t) \}. \quad (3.20)$$

Adding (3.16)-(3.20) together, we get

$$\begin{aligned} &\frac{1}{2} \frac{d}{dt} \left\{ \|\psi\|_{\Omega_i}^2 + \frac{1}{2} \left(\xi_0^3 \|\phi_1\|_{[0, L]}^2 + \eta_0^3 \|\phi_2\|_{[0, L]}^2 \right) + \frac{\xi_0^3}{8\eta_0^3} |\Phi_1|^2 + \frac{\eta_0^3}{8\xi_0^3} |\Phi_2|^2 \right\} \\ &= -3 \left(\xi_0 \|\psi\|_{[0, L]}^2 + \eta_0 \|\psi\|_{[0, L]}^2 + \frac{\xi_0^3\eta_0}{2} |\phi_1|^2 + \frac{\eta_0^3\xi_0}{2} |\phi_2|^2 \right) \\ &\quad + 2\text{Re} \left\{ \xi_0^3 \int_0^L \bar{\psi} \phi_1 + \eta_0^3 \int_0^L \bar{\psi} \phi_2 \right\} + 2\text{Im} \left\{ \xi_0^3 \int_0^L \psi \bar{\phi}_1 + \eta_0^3 \int_0^L \psi \bar{\phi}_2 \right\} \\ &\quad + \frac{1}{2} \left(\text{Re} \{ \xi_0^3 \bar{\phi}_1 \Phi_1 + \eta_0^3 \bar{\phi}_2 \Phi_2 \} + \text{Im} \{ \xi_0^3 (\phi_1 + \phi_2) \bar{\Phi}_1 + \eta_0^3 (\phi_1 + \phi_2) \bar{\Phi}_2 \} \right). \end{aligned} \quad (3.21)$$

Using $|\text{Re}(Z)| + |\text{Im}(Z)| \leq \sqrt{2} |Z|$, $|\text{Re}(Z)| \leq |Z|$, $|\text{Im}(Z)| \leq |Z|$, Hölder inequality and the

ϵ inequality, we have

$$\begin{aligned}
A &\equiv 2\operatorname{Re} \left\{ \xi_0^3 \int_0^L \bar{\psi} \phi_1 + \eta_0^3 \int_0^L \bar{\psi} \phi_2 \right\} + 2\operatorname{Im} \left\{ \xi_0^3 \int_0^L \psi \bar{\phi}_1 + \eta_0^3 \int_0^L \psi \bar{\phi}_2 \right\} \\
&\quad + \frac{1}{2} \left(\operatorname{Re} \{ \xi_0^3 \bar{\phi}_1 \Phi_1 + \eta_0^3 \bar{\phi}_2 \Phi_2 \} + \operatorname{Im} \{ \xi_0^3 (\phi_1 + \phi_2) \bar{\Phi}_1 + \eta_0^3 (\phi_1 + \phi_2) \bar{\Phi}_2 \} \right) \\
&\leq 2\sqrt{2}\xi_0^3 \|\psi\|_{[0,L]} \|\phi_1\|_{[0,L]} + 2\sqrt{2}\eta_0^3 \|\psi\|_{[0,L]} \|\phi_2\|_{[0,L]} \\
&\quad + \frac{\sqrt{2}}{2} \xi_0^3 |\phi_1| |\Phi_1| + \frac{\sqrt{2}}{2} \eta_0^3 |\phi_2| |\Phi_2| + \xi_0^3 |\phi_2| |\Phi_1| + \eta_0^3 |\phi_1| |\Phi_2| \\
&\leq 3 \left(\xi_0 \|\psi\|_{[0,L]}^2 + \eta_0 \|\psi\|_{[0,L]}^2 + \frac{\xi_0^3 \eta_0}{2} |\phi_1|^2 + \frac{\eta_0^3 \xi_0}{2} |\phi_2|^2 \right) \\
&\quad + \frac{8}{3} \xi_0^5 \|\phi_1\|_{[0,L]}^2 + \frac{8}{3} \eta_0^5 \|\phi_2\|_{[0,L]}^2 + \frac{2\xi_0^3}{\eta_0} |\Phi_1|^2 + \frac{2\eta_0^3}{\xi_0} |\Phi_2|^2 \\
&\leq 3 \left(\xi_0 \|\psi\|_{[0,L]}^2 + \eta_0 \|\psi\|_{[0,L]}^2 + \frac{\xi_0^3 \eta_0}{2} |\phi_1|^2 + \frac{\eta_0^3 \xi_0}{2} |\phi_2|^2 \right) \\
&\quad + c \left(\|\phi_1\|_{[0,L]}^2 + \|\phi_2\|_{[0,L]}^2 + |\Phi_1|^2 + |\Phi_2|^2 \right), \tag{3.22}
\end{aligned}$$

where $c = \max\{8\xi_0^5/3, 8\eta_0^5/3, 2\xi_0^3/\eta_0, 2\eta_0^3/\xi_0\}$. Inserting the inequality (3.22) into (3.22), we obtain

$$\begin{aligned}
&\frac{d}{dt} \left\{ \|\psi\|_{\Omega_i}^2 + \frac{1}{2} \left(\xi_0^3 \|\phi_1\|_{[0,L]}^2 + \eta_0^3 \|\phi_2\|_{[0,L]}^2 \right) + \frac{\xi_0^3}{8\eta_0^3} |\Phi_1|^2 + \frac{\eta_0^3}{8\xi_0^3} |\Phi_2|^2 \right\} \\
&\leq 2c \left(\|\phi_1\|_{[0,L]}^2 + \|\phi_2\|_{[0,L]}^2 + |\Phi_1|^2 + |\Phi_2|^2 \right) \tag{3.23}
\end{aligned}$$

Applying Gronwall's inequality to (3.23) leads us to (3.14). This completes the proof. \square

Theorem 3.1 shows the stability in the presence of LABCs on Γ_e , Γ_n and corner C_{NE} . Similarly, the stability in the presence of LABCs on other boundaries and corners can be straightforwardly achieved. It should be pointed out that the parameters ξ_0 and η_0 are considered as fixed positive finite constants in Theorem 3.1. In fact, the values of ξ_0 and η_0 are often chosen such that they are close to the group velocity of the wave, hence the parameters are finite and positive. If the weighted wave number selection approach (see (A.3)) is used to adaptively choose the parameters ξ_0 and η_0 . $\eta_0(x, t)$ and $\xi_0(y, t)$ will be not only functions of time t , but also functions of variable x and y , respectively. In practical calculations, it is expensive to compute $\eta_0(x, t)$ and $\xi_0(y, t)$ at every grid point. Alternatively, for any fixed time t , we only compute $\eta_0(x_i, t)$ (or $\xi_0(y_j, t)$) at one fixed grid point x_i (or y_j), then use $\eta_0(x_i, t)$ and $\xi_0(y_j, t)$ as the values of other points on the same artificial boundary. Thus the parameters ξ_0 and η_0 are only functions of time t in practical computations, for which, the stability can also be achieved by changing a few terms in the proof.

4. Discretization and Numerical Examples

In this section, we present numerical discretizations of the IBV problem of one dimension with boundary conditions \mathcal{LLABC} or \mathcal{LABC} . Extensions to two dimensional discretizations are

straightforward. Let J and M be positive integers, $h = (x_r - x_l)/J$ be the spatial step size, and $\Delta t = T/M$ be the time step size. Let

$$t_n = n\Delta t, \quad x_j = x_l + jh, \quad \psi_j^n \sim \psi(x_j, t_n), \quad \psi_j^{n+\frac{1}{2}} = \frac{\psi_j^{n+1} + \psi_j^n}{2},$$

$$D_x^2 \psi_j^n = \frac{\psi_{j-1}^n - 2\psi_j^n + \psi_{j+1}^n}{h^2}, \quad D_x \psi_j^n = \frac{\psi_{j+1}^n - \psi_{j-1}^n}{2h}, \quad f(|\psi_j^{n+1}|) = f(|\psi_j^{n+1}|, x_j, t_{n+1}).$$

For the model equation, Crank-Nicolson-type finite difference scheme [35] is employed,

$$i \frac{\psi_j^{n+1} - \psi_j^n}{\Delta t} + D_x^2 \frac{\psi_j^{n+1} + \psi_j^n}{2} - f(|\psi_j^{n+\frac{1}{2}}|) \frac{\psi_j^{n+1} + \psi_j^n}{2} = 0.$$

This scheme is implicit, and an iterative strategy is performed by replacing $f(|\psi_j^{n+1}|)$ with $f((|\psi_j^{n+1}|)^k)$, where the superscript k represents the k -th iteration at each time step and the data for the initial iteration step are given by $(\psi_j^{n+1})^0 = \psi_j^n$. The stop criteria is $\max_{0 \leq j \leq J} |(\psi_j^{n+1})^{k+1} - (\psi_j^{n+1})^k| \leq \epsilon := 10^{-12}$. We introduce two unknown ghost points x_{-1} and x_{J+1} , and denote x_s the grid points at the artificial boundaries with $s = 0$ or J . The \mathcal{LABC} s are discretized by

$$(-D_x \pm 3ik_0) \frac{\psi_s^{n+1} - \psi_s^n}{\Delta t} + (3ik_0^2 D_x \pm k_0^3) \psi_s^{n+\frac{1}{2}}$$

$$= \left[f(|\psi_s^{n+\frac{1}{2}}|) (iD_x \pm 3k_0) + iD_x f(|\psi_s^{n+\frac{1}{2}}|) \right] \psi_s^{n+\frac{1}{2}},$$

where the plus sign in “ \pm ” corresponds to the right boundary $s = J$ and the minus sign corresponds to the left boundary $s = 0$. The \mathcal{LLABC} s are discretized by

$$(-D_x \pm 3ik_0) \frac{\psi_s^{n+1} - \psi_s^n}{\Delta t} + (3ik_0^2 D_x \pm k_0^3) \psi_s^{n+\frac{1}{2}} = f(|\psi_s^{n+\frac{1}{2}}|) (iD_x \pm 3k_0) \psi_s^{n+\frac{1}{2}}.$$

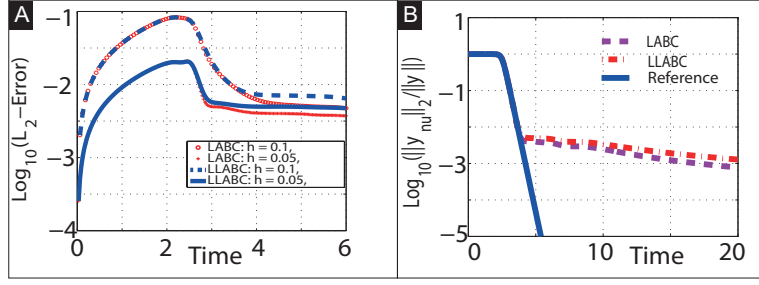
Now numerical examples are given to demonstrate the performance and the numerical stability of \mathcal{LABC} and \mathcal{LLABC} . In examples 1, 2 and 3, we consider one-dimensional case by investigating different nonlinearities. In example 4, we consider two-dimensional case by modeling the expansion of a Bose-Einstein condensate composed of waves with different group velocities.

Example 4.1. A focusing effect of the cubic nonlinearity is considered by taking $f(|\psi|, x, t) = -2|\psi|^2$. Its exact one-soliton solution has the following form

$$\psi(x, t) = A \operatorname{sech}(Ax - 2ABt) e^{iBx + i(A^2 - B^2)t},$$

where A and B are real parameters: A represents the amplitude of the wavefield and B the velocity of the soliton. In this example, we investigate the quantitative differences between \mathcal{LABC} and \mathcal{LLABC} . In the calculation, we use the parameters $A = 1, B = 2, [x_l, x_r] = [-10, 10], k_0 = 2.0$, and final time $T = 6.0$. The wave propagates into the positive-direction with speed $B = 2$, the boundary condition will have a good performance when the parameter k_0 is very close to the speed. Here and below, we will choose k_0 close to the speed of the wave. In order to evaluate the approximate accuracy of the reduced problems with absorbing boundary conditions, the *normalized* L^2 -error defined by

$$\frac{\|\psi_{nu} - \psi_{exa}\|_{2, [x_l, x_r]}}{\|\psi_0\|_{2, [x_l, x_r]}}$$

Fig. 4.1. $\log_{10}(L_2\text{-errors})$ (panel A) and Normalized L_2 -norm (panel B).Table 4.1: The L_2 -error and convergence order by using $\mathcal{L}ABC$ and $\mathcal{L}\mathcal{L}ABC$ at $T = 3$.

	$\Delta x = 0.2$	order	$\Delta x = 0.1$	order	$\Delta x = 0.05$	order
$\mathcal{L}ABC$	1.132e-1	–	2.694e-2	2.290	7.038e-3	1.936
$\mathcal{L}\mathcal{L}ABC$	1.141e-1	–	2.917e-2	2.274	8.151e-3	1.840

is used to characterize the error between the exact solution ψ_{exa} and the numerical solution ψ_{nu} of the reduced problem.

Panel A of Fig. 4.1 shows the $\log_{10}(L_2\text{-errors})$ versus time $t \leq 6$ with $h = 0.1, \Delta t = 0.01$ and their refined meshes. The L_2 -error computed by $\mathcal{L}ABC$ is smaller than the one by $\mathcal{L}\mathcal{L}ABC$ when $t > 4$. The long-time computation is showed in panel B of Fig. 4.1 with $h = 0.05, \Delta t = 0.005$, where the *normalized* L_2 -norm of numerical solution ψ_{nu} defined by $\frac{\|\psi_{nu}\|_{2,[x_l,x_r]}}{\|\psi_0\|_{2,[x_l,x_r]}}$. We terminates the calculation at $t = 20$. No energy growth is observed, which implies the stability of our $\mathcal{L}ABC$ and $\mathcal{L}\mathcal{L}ABC$. Table 4.1 shows the time-dependent errors in L_2 -norm and convergence order at $T = 3$ by taking $\Delta t = h^2$. The time-dependent error in L^2 -norm is defined by

$$\frac{1}{M} \sum_{n=1}^M \|\psi_{nu}(t_n) - \psi_{exa}(t_n)\|_{2,[x_l,x_r]}.$$

From Fig. 4.1 and Table 4.1, both boundary conditions $\mathcal{L}ABC$ and $\mathcal{L}\mathcal{L}ABC$ are stable, and $\mathcal{L}ABC$ has better performance than $\mathcal{L}\mathcal{L}ABC$ by comparing the errors in L^2 -norm.

Example 4.2. To model the expansion of a Bose-Einstein condensate composed of waves with different group velocities, we take nonlinearity

$$f(|\psi|, x, t) = 2|\psi|^2 + V(x),$$

and the Gaussian initial function $\psi_0 = e^{-0.1x^2}$, and the potential $V(x) = e^{-0.5x^2}$. This represents a nonlinear wave for repulsive interaction. In the calculation, the parameters are taken by $k_0 = 2, h = 10^{-2}, \Delta t = 2 \times 10^{-3}, T = 6, [x_l, x_r] = [-15, 15]$. Panels A and B of Fig. 4.2 plot numerical solutions $|\psi|$ generated by $\mathcal{L}ABC$ and $\mathcal{L}\mathcal{L}ABC$ at time $t = 2, 4, 6$. There is no obvious reflected wave by the boundary conditions, which implies that both $\mathcal{L}ABC$ and $\mathcal{L}\mathcal{L}ABC$ perform well and are stable.

Example 4.3. The nonlinearity is taken by

$$f(|\psi|, x, t) = -2|\psi|^4 - 2|\psi|^2$$

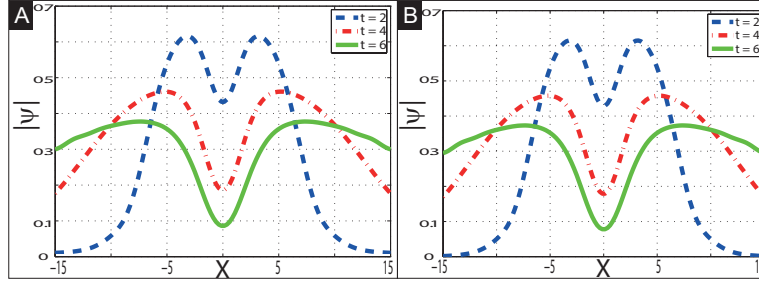


Fig. 4.2. The numerical solutions at different time: $\mathcal{L}ABC$ (panel A) and $\mathcal{L}LABC$ (panel B).

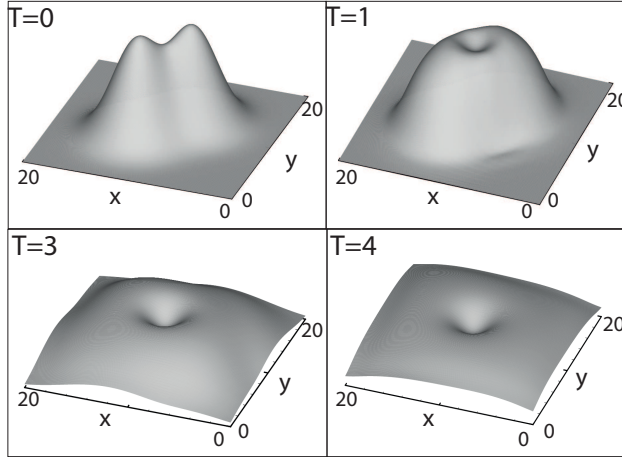


Fig. 4.3. The evolutions of numerical solutions calculated by $\mathcal{L}ABC$ at different time.

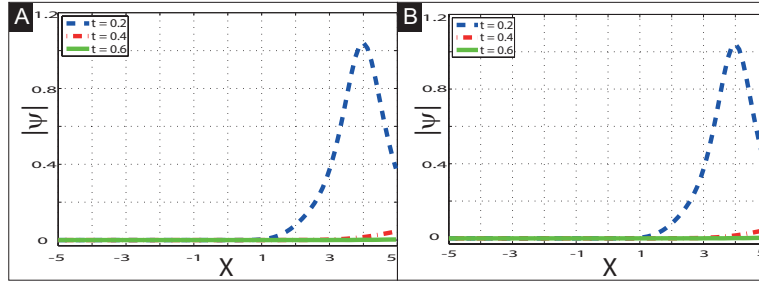


Fig. 4.4. The numerical solutions at different time: $\mathcal{L}ABC$ (panel A) and $\mathcal{L}LABC$ (panel B).

and initial value $\psi_0 = e^{10ix - x^2}$. The parameters are taken by $k_0 = 10, h = 5 \times 10^{-3}, \Delta t = 5 \times 10^{-4}, [x_l, x_r] = [-5, 5], T = 2$. Panels A and B of Fig. 4.4 show the evolutions of numerical solutions respectively obtained by $\mathcal{L}ABC$ and $\mathcal{L}LABC$ at time $t = 0.2, 0.4, 0.6$. Both $\mathcal{L}ABC$ and $\mathcal{L}LABC$ have a good performance and are stable.

Example 4.4. This is a two-dimensional example. The nonlinear term is taken by

$$f(|\psi|, x, y, t) = 2|\psi|^2 + V(x, y)$$

with the potential $V(x, y) = e^{-0.5(x-10)^2 - 0.5(y-10)^2}$. The initial wave is given by overlapping

two Gaussian pulses (see Fig. 4.3 for case $T = 0$)

$$\psi(x, y, 0) = e^{-0.1(x-8)^2 - 0.1(y-8)^2} + e^{-0.1(x-12)^2 - 0.1(y-12)^2}.$$

This nonlinear wave interacts repulsively and will impinge on all artificial boundaries and corners. In the calculation, we take $L = 20$, $\Delta x = \Delta y = 0.05$ and $\Delta t = 0.005$, $\xi_0 = \eta_0 = 2.0$. Fig. 4.3 represents the evolution of the numerical solution at different snapshots ($t = 1, 3, 4$). One can see that no obvious reflections appear near the boundaries and corners, which imply that the boundary conditions are stable and work well.

5. Conclusions

The stability of the reduced problem with LABCs constructed by the unified approach for nonlinear Schrödinger equations are studied in this paper. By introducing auxiliary variables to reduce the boundary conditions with high-order mixed derivatives into a family of equations with lower-order derivatives, we proved that the IBV problems with the boundary conditions (\mathcal{LLABCs}) constructed in [30, 31] are stable in L^2 -norm. Furthermore, we extend the strategy of auxiliary variables to two-dimensional case and obtain the corresponding energy estimate by carefully dealing with the boundary conditions at corners. For one-dimensional case, we also consider that the parameters k_0 change with time t when the adaptive algorithm is implemented in the Appendix. The framework of this paper is still valid to prove the stability of the boundary conditions \mathcal{LLABCs} with adaptive k_0 . For two-dimensional case, ξ_0 and η_0 are possible to be functions of spatial x and y , the stability analysis will be very complicate. In practical computations where the parameters ξ_0 and η_0 are only functions of time t , the energy estimate can also be obtained. In this paper, we also discuss a variety of boundary conditions \mathcal{LABCs} , many numerical examples showed that \mathcal{LABCs} are stable numerically and even have a better performance (see Fig. 4.1 and Table 4.1) than \mathcal{LLABCs} . Although the numerical simulations show that the solutions of the reduced problem can well approximate the original solution, the theoretical approximate accuracy still remain open. The rigorous mathematical analysis of the accuracy of the LABCs would be an interesting topic for the future research.

In the future, we will base on the results of energy estimate in this paper to consider the nonlinear Schrödinger equation in semiclassical regime on unbounded domain:

$$i\varepsilon\partial_t\psi(\mathbf{x}, t) = -\varepsilon^2\Delta\psi(\mathbf{x}, t) + V(\mathbf{x})\psi(\mathbf{x}, t) + f(|\psi(\mathbf{x}, t)|^2)\psi(\mathbf{x}, t), \quad \mathbf{x} \in \mathbb{R}^d, \quad t > 0,$$

with the ‘‘scaled’’ Planck constant $0 < \varepsilon \ll 1$. In this situation, the wave function ψ becomes oscillatory of wave length $\mathcal{O}(\varepsilon)$. This means one has to work on a large computational domain that contains thousands to millions of wavelengths, and each of them needs to be resolved if direct numerical methods are applied. For example, a mesh size of $\mathcal{O}(\varepsilon)$ is required when using the time-splitting spectral method [36]. We will analyze the relationship between energy bound and ε by using the technique in this paper, then will propose an asymptotic method based on frozen Gaussian approximation for the case of ε being small (refer to [37] for linear Schrödinger equation in semiclassical regime).

Acknowledgements. This research is supported by NSFC (91430216 and U1530401), the Chinese Ministry of Education (NCET-09-0556), the Scientific Research Starting Foundation for Returned Overseas Chinese Scholars, and the GRF (HKBU 12302414) of Hong Kong.

Appendix: Adaptive algorithm for wavenumber parameter

LABCs include parameter $k_0 = \sqrt{\omega_0}$ to be determined. This parameter is related to the frequency of the wave impinging on the artificial boundary. In order to obtain the local structure of the wave in the frequency domain, the Gabor transform was introduced in [29], expressed as,

$$\hat{\psi}(k, t) = \int_{x_l}^{x_r} \mathbf{1}_{[x_r - \mathbf{b}, x_r]} \psi(x, t) e^{-ikx} = \int_{x_l - \mathbf{b}}^{x_r} \psi(x, t) e^{-ikx},$$

with \mathbf{b} denoting the window width. One reasonable choice of wavenumber k_0 is to take the mode such that its spectrum is the maximum, i.e.,

$$|\hat{\psi}(k_0, t)| = \sup_{k \geq 0} \left\{ |\hat{\psi}(k, t)| \right\}. \quad (\text{A.1})$$

Another choice is to use the energy-weighted wavenumber approach

$$k_0 = \frac{\int_0^\infty |\hat{\psi}(k, t)|^m k dk}{\int_0^\infty |\hat{\psi}(k, t)|^m dk} \quad (\text{A.2})$$

with m a positive real number. The authors in [29] suggested to use $m = 4$. In many practical calculations, the wavenumber k_0 by formula (A.2) is more efficient and accurate than (A.1). In fact, the cost of comparing all magnitudes of Fourier modes is expensive. On the other hand, when two Fourier modes are both dominant, a medial value of these two different wavenumbers instead of choosing one of them is better to minimize the reflection.

For two dimensions, the algorithm of determining ξ_0 and η_0 can be extended straightforwardly from that of one dimension. For example, to obtain the wavenumber $\xi_0(y, t)$ on the west boundary Γ_w , we could use the Gabor transform in x -direction:

$$\hat{\psi}(\xi, y, t) = \int_{x_w}^{x_w + \mathbf{b}(y)} \psi(x, y, t) e^{-i\xi x} dx,$$

where the window length $\mathbf{b}(y)$ is a function of y . The wavenumber ξ_0 can be obtained by

$$\xi_0(y, t) = \frac{\int_0^\infty |\hat{\psi}(\xi, y, t)|^m \xi d\xi}{\int_0^\infty |\hat{\psi}(\xi, y, t)|^m d\xi}. \quad (\text{A.3})$$

The parameters on other artificial boundaries can be calculated by the same way.

References

- [1] C. Sulem, P. Sulem, *The Nonlinear Schrödinger Equation: Self-Focusing and Wave Collapse*, Springer, 1999.
- [2] G. Agrawal, *Nonlinear Fiber Optics*, 3rd Ed., Academic Press, San Diego, 2001.
- [3] L. P. Pitaevskii, S. Stringari, *Bose-Einstein Condensation*, Oxford University Press, Oxford, 2003.
- [4] X. Antoine, W. Bao and C. Besse, Computational methods for the dynamics of the nonlinear Schrödinger/Gross-Pitaevskii equations, *Comput. Phys. Commun.*, **184**:12 (2013), 2621-2633.
- [5] W. Bao, D. Jaksch, P. Markowich, Numerical solution of the Gross-Pitaevskii equation for Bose-Einstein condensation, *J. Comput. Phys.*, **187** (2003), 318-342.
- [6] M.A.L. Marques, E.K.U. Gross, Time-dependent density functional theory, *Annu. Rev. Phys. Chem.*, **55** (2004), 427-455.

- [7] T. Hagstrom, S.Lau, Radiation boundary conditions for Maxwell's equations: A review of accurate time-domain formulations, *J. Comput. Math.*, **25** (2007), 305–336.
- [8] X. Antoine, A. Arnold, C. Besse, M. Ehrhardt, A. Schädle, A review of transparent and artificial boundary conditions techniques for linear and nonlinear Schrödinger equations, *Commun. Comput. Phys.*, **4** (2008), 729–796.
- [9] H. Han, X. Wu, Artificial Boundary Method-Numerical Solutions of Partial Differential Equations on Unbounded Domains, Tsinghua University and Springer Publisher, 2013.
- [10] Berenger J P. A perfectly matched layer for the absorption of electromagnetic waves. *J. Comput. Phys.*, **114**:2 (1994), 185-200.
- [11] Bao G, Chen Z, Wu H. Adaptive finite-element method for diffraction gratings. *JOSA A*, **22**:6 (2005), 1106-1114.
- [12] Chen Z, Zheng W. Convergence of the uniaxial perfectly matched layer method for time-harmonic scattering problems in two-layered media. *SIAM J. Num. Anal.*, **48**:6 (2006), 2158-2185.
- [13] C. Farrell, U. Leonhardt, The perfectly matched layer in numerical simulations of nonlinear and matter waves, *J. Opt. B: Quantum Semiclass. Opt.*, **7** (2005), 1-4.
- [14] C. Zheng, A perfectly matched layer approach to the nonlinear Schrödinger wave equations, *J. Comput. Phys.*, **227** (2007), 537–556.
- [15] D. Neuhauser, M. Baer, The time-dependent Schrödinger equation: application of absorbing boundary conditions, *J. Chem. Phys.*, **90** (1989), 4351–4355.
- [16] Z.Z. Sun, X. Wu, The stability and convergence of a difference scheme for the Schrödinger equation on an infinite domain by using artificial boundary conditions, *J. Comput. Phys.*, **214** (2006), 209–223.
- [17] S.D. Jiang, L. Greengard, Fast evaluation of nonreflecting boundary conditions for the Schrödinger equation in one dimension, *Comput. Math. Appl.*, **47** (2004), 955–966.
- [18] H. Han, Z. Huang, Exact artificial boundary conditions for Schrödinger equation in R^2 , *Commun. Math. Sci.*, **2** (2004), 79–94.
- [19] H. Han, D. Yin, Z. Huang, Numerical solutions of Schrödinger equations in R^3 , *Numer. Meth. Partial Diff. Eq.*, **23** (2007), 511–533.
- [20] C. Zheng, Exact nonreflecting boundary conditions for one-dimensional cubic nonlinear Schrödinger equations, *J. Comput. Phys.*, **215** (2006), 552–565.
- [21] M. Ehrhardt, C.X. Zheng, Exact artificial boundary conditions for problems with periodic structures, *J. Comput. Phys.*, **227** (2008), 6877–6894.
- [22] M. Ehrhardt, H. Han, C.X. Zheng, Numerical simulation of waves in periodic structures, *Commun. Comput. Phys.*, **5** (2009), 849–870.
- [23] X. Antoine, C. Besse, S. Descombes, Artificial boundary conditions for one-dimensional cubic nonlinear Schrödinger equations, *SIAM J. Numer. Anal.*, **43** (2006), 2272–2293.
- [24] X. Antoine, C. Besse, P. Klein, Absorbing boundary conditions for the one-dimensional Schrödinger equation with an exterior repulsive potential, *J. Comput. Phys.*, **228** (2009), 312–335.
- [25] X. Antoine, C. Besse, P. Klein, Absorbing boundary conditions for general nonlinear Schrödinger equations, *SIAM J. Sci. Comput.*, **33** (2011), 1008-1033.
- [26] B. Engquist, A. Majda, Absorbing boundary conditions for the numerical simulation of waves, *Math. Comput.*, **31** (1977), 629–651.
- [27] B. Engquist and A. Majda, Radiation boundary conditions for acoustic and elastic wave calculations, *Comm. Pure Appl. Math.*, **32** (1979), 314–358.
- [28] Z. Xu, H. Han, Absorbing boundary conditions for nonlinear Schrödinger equations, *Phys. Rev.*, E **74** (2006), 037704.
- [29] Z. Xu, H. Han, X. Wu, Adaptive absorbing boundary conditions for Schrödinger-type equations: application to nonlinear and multi-dimensional problems, *J. Comput. Phys.*, **225** (2007), 1577–1589.

- [30] J. Zhang, Z. Xu, X. Wu, Unified approach to split absorbing boundary conditions for nonlinear Schrödinger equations, *Phys. Rev.*, E **78** (2008), 026709.
- [31] J. Zhang, Z. Xu, X. Wu, Unified approach to split absorbing boundary conditions for nonlinear Schrödinger equations: Two dimensional case, *Phys. Rev.*, E **79** (2009), 046711.
- [32] H. Brunner, X. Wu, J. Zhang, Computational solution of blow-up problems for semilinear parabolic PDEs on unbounded domains, *SIAM J. Sci. Comput.*, **31** (2010), 4478–4496.
- [33] J.-P. Kuska, Absorbing boundary conditions for the Schrödinger equation on finite intervals, *Phys. Rev.*, B **46** (1992), 5000.
- [34] G. Strang, On the construction and comparison of difference schemes, *SIAM J. Numer. Anal.*, **5** (1968), 506–517.
- [35] A. Durán, J.M. Sanz-Serna, The numerical integration of relative equilibrium solution. The non-linear Schrödinger equation, *IMA J. Numer. Anal.*, **20**:2 (2000), 235–261.
- [36] W. Bao, S. Jin and P.A. Markowich, On time-splitting spectral approximations fro the Schrödinger equation in the semiclassical regime, *J. Comput. Phys.*, **175**:2 (2002), 487-524.
- [37] X. Yang and J. Zhang, Computation of the Schrödinger equation in the semiclassical regime on unbounded domain, *SIAM J. Numer. Anal.*, **52**:2 (2014), 808-831.